

Deep-learning-assisted optical communication with discretized state space of structured light

Minyang Zhang(张敏洋), Dong-Xu Chen(陈东旭), Pengxiang Ruan(阮鹏祥), Jun Liu(刘俊), Dong-Zhi Fu(付栋之), Jun-Long Zhao(赵军龙), and Chui-Ping Yang(杨垂平)

Citation: Chin. Phys. B, 2024, 33 (**12**): 120304. DOI: 10.1088/1674-1056/ad8553
Journal homepage: http://cpb.iphy.ac.cn; http://iopscience.iop.org/cpb

What follows is a list of articles you may be interested in

Variational data encoding and correlations in quantum-enhanced machine learning

Ming-Hao Wang(王明浩) and Hua Lü(吕桦)
Chin. Phys. B, 2024, 33 (**9**): 090307. DOI: 10.1088/1674-1056/ad5c3b

Machine-learning-assisted efficient reconstruction of the quantum states generated from the Sagnac polarization-entangled photon source

Menghui Mao(毛梦辉), Wei Zhou(周唯), Xinhui Li(李新慧), Ran Yang(杨然), Yan-Xiao Gong(龚彦晓), and Shi-Ning Zhu(祝世宁)
Chin. Phys. B, 2024, 33 (**8**): 080301. DOI: 10.1088/1674-1056/ad51f7

Recurrent neural network decoding of rotated surface codes based on distributed strategy

Fan Li(李帆), Ao-Qing Li(李熬庆), Qi-Di Gan(甘启迪), and Hong-Yang Ma(马鸿洋)
Chin. Phys. B, 2024, 33 (**4**): 040307. DOI: 10.1088/1674-1056/ad2bef

Realization of quantum permutation algorithm in high dimensional Hilbert space

Dong-Xu Chen(陈东旭), Rui-Feng Liu(刘瑞丰), Pei Zhang(张沛), Yun-Long Wang(王云龙), Hong-Rong Li(李宏荣), Hong Gao(高宏), Fu-Li Li(李福利)
Chin. Phys. B, 2017, 26 (**6**): 060305. DOI: 10.1088/1674-1056/26/6/060305

Free-space measurement-device-independent quantum-key-distribution protocol using decoy states with orbital angular momentum

Wang Le (王乐), Zhao Sheng-Mei (赵生妹), Gong Long-Yan (巩龙延), Cheng Wei-Wen (程维文)
Chin. Phys. B, 2015, 24 (**12**): 120307. DOI: 10.1088/1674-1056/24/12/120307

Deep-learning-assisted optical communication with discretized state space of structured light

Minyang Zhang(张敏洋)[1], Dong-Xu Chen(陈东旭)[2,3,†], Pengxiang Ruan(阮鹏祥)[1], Jun Liu(刘俊)[1], Dong-Zhi Fu(付栋之)[4], Jun-Long Zhao(赵军龙)[2], and Chui-Ping Yang(杨垂平)[5,‡]

[1] *School of Science, Jiangsu University of Science and Technology, Zhenjiang* 212003, *China*
[2] *Quantum Information Research Center, Shangrao Normal University, Shangrao* 334001, *China*
[3] *Jiangxi Province Key Laboratory of Applied Optical Technology (*2024SSY03051*), Shangrao Normal University, Shangrao* 334001, *China*
[4] *School of Cable Engineering, Henan Institute of Technology, Xinxiang* 453003, *China*
[5] *School of Physics, Hangzhou Normal University, Hangzhou* 311121, *China*

(Received 6 August 2024; revised manuscript received 8 October 2024; accepted manuscript online 10 October 2024)

The rich structure of transverse spatial modes of structured light has facilitated their extensive applications in quantum information and optical communication. The Laguerre–Gaussian (LG) modes, which carry a well-defined orbital angular momentum (OAM), consist of a complete orthogonal basis describing the transverse spatial modes of light. The application of OAM in free-space optical communication is restricted due to the experimentally limited OAM numbers and the complex OAM recognition methods. Here, we present a novel method that uses the advanced deep learning technique for LG modes recognition. By discretizing the spatial modes of structured light, we turn the OAM state regression into classification. A proof-of-principle experiment is also performed, showing that our method effectively categorizes OAM states with small training samples and the accuracy exceeds 99% from three-dimensional (3D) to fifteen-dimensional (15D) space. By assigning each category a classical information, we further apply our approach to an image transmission task, achieving a transmission accuracy of 99.58%, which demonstrates the ability to encode large data with low OAM number. This work opens up a new avenue for achieving high-capacity optical communication with low OAM number based on structured light.

Keywords: orbital angular momentum, machine learning, optical communication

PACS: 03.67.–a, 42.50.Tx, 42.79.Sz **DOI:** 10.1088/1674-1056/ad8553

1. Introduction

The orbital angular momentum (OAM) of light, characterized by its distinctive helical phase front $e^{i\ell\phi}$, has facilitated a pivotal breakthrough in the field of optics. The advent of OAM plays a crucial role in advancing the frontiers of many fields, such as optical communication, quantum information, and quantum computation. The OAM of light offers advantages over the well-studied spin angular momentum, i.e., the polarization of light, due to the inherent high dimensional peculiarity. For example, it has been shown that the OAM of light can be applied to realize high-dimensional quantum communication with larger alphabet and higher security.[1–6] High-dimensional quantum entangled states can be generated with the OAM, which show larger violation of Bell nonlocality.[7–9]

In the field of telecommunications, OAM is crucial for the development of high-capacity optical networks, especially in the enhancement of data transmission capabilities. Its unique ability to handle large data streams offers potential solutions to bandwidth limitations and efficiency challenges in fiber optical communication systems. Most importantly, as a cornerstone of high-dimensional quantum information processing, OAM has facilitated significant advancements in quantum computing and quantum encryption technology. The significance of OAM in these aspects is becoming ever more paramount, due to the increasing focus on higher bandwidth and denser information density nowadays.

Previous works on the OAM of light focused on the generation and measurement of the OAM states. An OAM state with large ℓ and a simple method to recognize the OAM state are preferred in practical applications. However, the quantum numbers ℓ of experimentally generated OAM states are limited due to the imperfections of experimental devices. In 2016, Zeilinger's group generated the OAM states with quantum numbers up to 10010 and realized quantum entanglement of these states.[10] On the other hand, the existing methods for measuring OAM states either cannot be applied in single photon level[11–14] or require complex measurement setups due to the high-dimension nature of OAM states.[15–23] Therefore, how to increase the channel capacity with limited OAM number is one active research area in OAM-based optical communication. Meanwhile, a flexible approach that can be adapted to the practical situations to recognize the OAM states is important for the applications of OAM.

Early applications of OAM in optical communica-

†Corresponding author. E-mail: chendx@sru.edu.cn
‡Corresponding author. E-mail: yangcp@hznu.edu.cn

© 2024 Chinese Physical Society and IOP Publishing Ltd

tion aimed to increase channel capacity through OAM multiplexing.[24–26] The OAM multiplexing technique treats OAM as one more degree of freedom in addition to other degrees of photons. Therefore, higher capacity could be achieved by exhausting available degrees of freedom of photons. However, only a subset of OAM states was used and the rich structure of the spatial modes was not fully harnessed. In recent years, the development of machine learning (ML) has promoted a new frontier in the research of photonic OAM. The enhanced capabilities of ML in data analysis and feature recognition open up novel avenues in the exploration for OAM beams, particularly in the recognition of OAM. Research in this field can be classified into two categories, classification and regression of photons' OAMs. Classification of photons' OAMs predicts the OAM values from a given list, while the regression of photons' OAMs predicts the OAM spectrum of an unknown state. In other words, classification of OAM states resolves the discretized OAM spectrum recognition task;[27–29] while regression of OAM states resolves the continuous OAM spectrum recognition task which requires more samples for training.[30–32]

There are various application of ML in OAM-based optical communication. For example, the ML technique has been applied in free-space optical communication to correct the deformation of the optical modes caused by turbulences.[33–37] Also, the ML technique has assisted the recognition of fractional optical vortex modes,[38–41] which opens a new way for high-capacity optical communication. In spite of the super-high resolution of fractional optical vortex modes (98% accuracy with OAM interval of 0.01[38]), the fractional optical vortex modes are not ideal in practical application since they quickly diffract due to the phase discontinuity. Moreover, the distortion of the fractional optical vortex modes in the generating process would affect the accuracy apparently.

In this work, we apply the ML technique in the OAM state recognition for high-capacity optical communication. We discretize transverse spatial modes of structured light into individual partitions. Then we use the ML technique to effectively classify the OAM states. In this way, we turn the OAM state regression into classification, thus reducing the requirement of training samples. For the OAM states in each partition, we assign them a classical information. In other words, quantum information is approximately represented by classical information. We further apply our method to an image transmission task, demonstrating the ability to encode large data with low OAM number.

The key idea of this work is the discretization of the state space of light's spatial modes, which has not been reported before. We further apply this idea to enhance the capacity of optical communication, which is different from the existing ways.[42–44] The spatial modes of light are fully harnessed by considering the azimuthal and radial indexes of LG modes, which transmit stably in free space. In addition, since the OAM states in each partition represent the same information, our method allows for imperfection of OAM states in the generating process. Our method aims to overcome the challenges associated with the experimental realization of the OAM states, particularly the limitations on the orders of the OAM states.

2. Methods

2.1. Dimension of the transverse spatial modes of structured light

The transverse structure of paraxial beams propagating in free space can be described by different classes of orthonormal sets. The Hermite–Gaussian (HG) modes and the Laguerre–Gaussian (LG) modes are two widely-studied classes used to describe the transverse structure of a light beam. It was shown that the LG modes and the HG modes could be transformed through unitary operations[45]

$$\mathrm{LG}_{n,m} = \sum_{k=0}^{N} \mathrm{i}^k b(n,m,k) \mathrm{HG}_{N-k,k}, \tag{1}$$

where

$$b(n,m,k) = \left(\frac{(N-k)!k!}{2^N n!m!}\right)^{1/2} \frac{1}{k!} \frac{\mathrm{d}^k}{\mathrm{d}t^k}[(1-t)^n(1+t)^m]_{t=0}, \tag{2}$$

and $N = n+m$ is the order of the optical mode. Here, the radial index p and the azimuthal index (i.e., the OAM number) ℓ of LG modes are $p = \min(n,m)$ and $\ell = n-m$, respectively. In this paper, we use the notation $\mathrm{LG}_{n,m}$ to denote LG modes in accordance with the HG modes for order $N = n+m$, while we use the notation $\mathrm{LG}(\ell,p)$ to explicitly denote the LG modes with OAM values ℓ and radial number p.

One can see from Eq. (1) that an LG beam can be decomposed into superposition of $N+1$ HG beams with the same order, and vice versa. Therefore, one could define the dimension of a subspace of the transverse mode $D = N+1$. In a subspace of dimension D, the LG modes and the HG modes could be transformed through unitary operations. For example, the $\mathrm{LG}(\ell,p)$ modes LG(2,0), LG($-$2,0), and LG(0,1) constitute a set of basis in a three-dimensional (3D) subspace, while the $\mathrm{HG}(m,n)$ modes HG(1,1), HG(2,0), and HG(0,2) constitute another set of basis.

Within the scope of OAM recognition research, most existing studies primarily set the radial index p to zero. While this simplification eases analysis, it overlooks the complexity arising from the combination of radial and azimuthal indexes. Here, we consider the complete spatial modes of structured light by taking account for the index p. By harnessing the complex spatial modes of structured light, we obtain a

higher dimension of the transverse modes than only utilizing the OAM index ℓ.

2.2. Discretization of the state space

A quantum state in an N-dimensional quantum space can be represented by a state vector of N elements. In quantum information, a d-state quantum system ($d > 2$) is called a qudit, while a 2-state quantum system is called a qubit. For a qubit, an arbitrary pure quantum state can be represented by a point on the surface of the Bloch sphere. Here, we divide the spherical surface into several regions, each of which contains many states. We assign each region with a classical state, i.e., all the states in the region represent the same classical information. In other words, a qubit is approximated to n classical bits, with 2^n being the number of the partitions of the spherical surface.

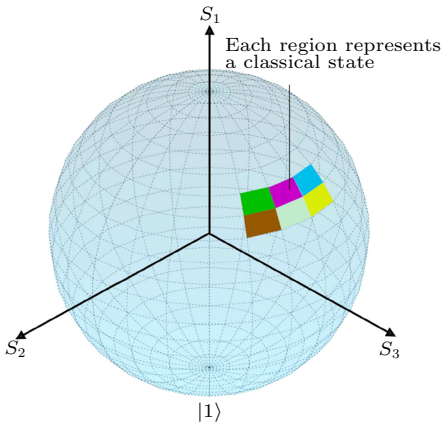


Fig. 1. Discretization of the Bloch sphere. The polar angle and the azimuthal angle are uniformly divided, thus the surface of the Bloch sphere is partitioned into several regions. Each region is endowed with a classical state.

A geometrical representation of such process is shown in Fig. 1. A general qubit state has the form

$$|\phi\rangle = \cos\frac{\theta}{2}|0\rangle + \sin\frac{\theta}{2}\mathrm{e}^{\mathrm{i}\varphi}|1\rangle, \tag{3}$$

where θ and φ are the polar angle and the azimuthal angle of the sphere. For example, we divide θ and φ into 8 regions, respectively. The spherical surface is thus discretized into 64 regions. Therefore, a qubit is approximated to 6 classical bits. For a higher dimensional quantum space, one can follow the same procedure to discretize the space into several regions.

The proposed discretization process in this work turns the OAM states regression into OAM states classification. Note that when the partitions of θ and φ go to infinity, the problem becomes dividing OAM states into infinite categories, which is equivalent to OAM state regression.

2.3. Deep learning model

We develop an OAM-recognition neural network using deep learning technique shown in Fig. 2, which is pivotal for managing intricate tasks like image recognition and classification.[38,46] Our study primarily concentrates on an enhanced version of a distinguished member of the residual network (ResNet) family,[47] the ResNet50. This version integrates the concept of residual blocks and skips connections, effectively tackling the issue of vanishing gradients often encountered during complex image training. Each residual block comprises a sequence of convolutional layers, particularly the BottleneckBlock units.[48] These units start with a 1×1 convolution to reduce data dimensions, followed by a 3×3 convolution for a comprehensive feature extraction, and conclude with another 1×1 convolution to restore the data dimensions. Moreover, our discretization model adopts the CrossEntropyLoss function, which combines log softmax and negative log-likelihood loss to accurately compute gradients. We have implemented the ReduceLROnPlateau scheduler for dynamic adjustment of the learning rate, adapting it based on trends in validation loss to mitigate overfitting risks. Additionally, our model incorporates data augmentation and dropout techniques to enhance its generalization across various OAM states.

Regarding the model's architecture, we have devised a novel two-stage structure specifically tailored for the systematic processing of optical OAM information. In the initial stage, the model conducts a broad categorization of fundamental layers, distinguishing between various OAM categories presented in optical images. The subsequent stage involves a detailed sub-classification based on the primary layer's categorization, focusing on subtle variations in phase

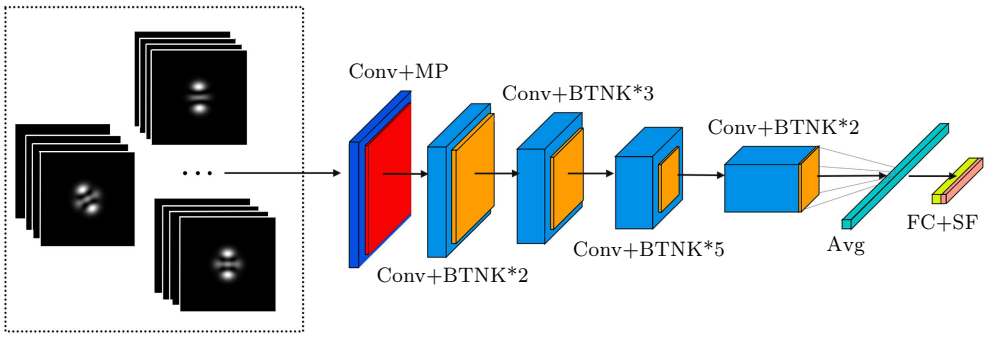


Fig. 2. Neural network model for OAM-recognition. The model architecture is based on an enhanced version of ResNet50. It includes convolutional layers (Conv) for feature extraction, batch normalization (BTNK) for stable training, max pooling (MP) for spatial reduction, fully connected layers (FC) for complex pattern learning, and softmax activation (SF) for multi-class classification.

weights within optical images. By leveraging the inherent advantages of existing datasets, our model divides the OAM-recognition classification task into two stages, effectively overcoming challenges commonly associated with complex and high-dimensional datasets. This approach achieves rapid and high-precision classification while also partially reducing computational costs.

3. Results

The experimental setup is shown in Fig. 3. A coherent beam emitting from a laser diode is coupled into a single mode fiber. Then the beam is expanded by a $4f$ lens system to fit the size of the spatial light modulator (SLM). The SLM is loaded with gratings which generate the desired optical fields. The reflected beam is filtered by an aperture to pick out the first-order diffraction beam which is finally recorded by a CCD camera. Examples of experimentally generated structured light in a three-dimensional space are shown in Fig. 3(b).

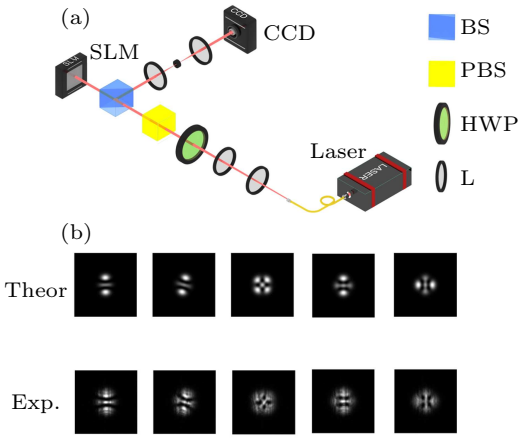


Fig. 3. (a) Sketch of the experimental setup. A coherent beam emits from a laser diode is expanded by a $4f$ system. Then the SLM is loaded with holograms to generated OAM states. Finally, a CCD camera captures the intensity profile. (b) Examples of the generated OAM states in a 3D space for six categories. SLM: spatial light modulator, HWP: half-wave plate, PBS: polarizing beam splitter, BS: beam splitter, L: lens.

The recorded images are then used for training. For a three-dimensional space, the basis states are LG(2,0), LG($-$2,0), and LG(0,1). A general quantum state in such a space has the following form:

$$|\psi\rangle = \alpha|\mathrm{LG}(2,0)\rangle + \beta|\mathrm{LG}(-2,0)\rangle + \gamma|\mathrm{LG}(0,1)\rangle, \quad (4)$$

where α, β, and γ are complex numbers which are normalized as $|\alpha|^2+|\beta|^2+|\gamma|^2=1$. In our experiment, we focus on the states with equal-weighted superposition, i.e., $\alpha = 1/\sqrt{3}$, $\beta = \mathrm{e}^{\mathrm{i}\varphi_1}/\sqrt{3}$, $\gamma = \mathrm{e}^{\mathrm{i}\varphi_2}/\sqrt{3}$. Due to the degeneracy of the intensity profile of the OAM states $|\pm\ell\rangle$, we confine φ_1 and φ_2 between 0 and π. We further divide φ_1 and φ_2 into 30 intervals. We fix $\varphi_1 = 0$ and change φ_2, then fix $\varphi_2 = 0$ and change φ_1. In this way, we obtain 60 categories for a three-dimensional space. For each category, we generate 100 random samples for the model training, which are segmented into a training set (80 images) and a validation set (20 images). For instance, for the first category with $\varphi_1 = 0$ and $\varphi_2 \in (0, \pi/30)$, the samples are obtained by loading holograms which generate the state $|\psi\rangle$ with φ_2 uniformly distributed between 0 and $\pi/30$. In Fig. 3(b), the values of φ_1 and φ_2 for the five samples are $(0.003, 0), (1.08, 0), (2.11, 0), (0, 0.005), (0, 1.06)$, respectively. We capture images of these states using a CCD camera and label them based on their OAM parameters. It is worth noting that one can extend the phase to the range $[0, 2\pi]$, with additional effort to break the degeneracy of the intensity profile of the states $|\pm\ell\rangle$ by taking one more picture.[30]

We first train the model using a theoretical dataset. For the validation process, we use a test set entirely composed of experimental data. We only achieve a relatively low validation accuracy of $80\% \pm 10\%$. Here, accuracy is defined as the ratio of the number of correct predictions to the total number of samples. Moreover, incorporating experimental images into the training set allows for a more accurate simulation of actual experimental conditions. Therefore, to enhance the model's robustness, we gradually increase the proportion of experimental images in the training set to 20%, 40%, 60%, and 80%, while the validation set consistently comprises of the experimental images only. The result is shown in Fig. 4. This incremental integration approach leads to a continuous improvement in accuracy, culminating in an optimal performance of 99.33% accuracy when both training and validation sets consist purely of the experimental data. Figures 5(a) and 5(b) show the training evolution through the epochs. The loss and the accuracy of the validation set and the training set both show the consistent trend across epochs. The model obtains a relatively stable performance after about epoch 20.

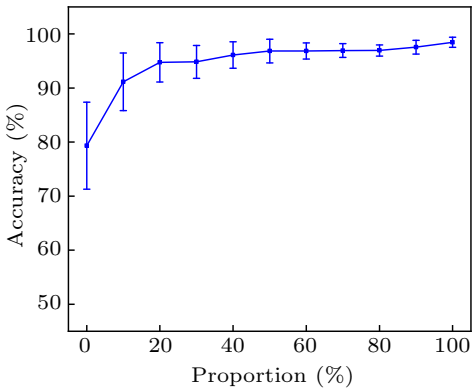


Fig. 4. Prediction accuracy versus proportion of experimental images in the training set.

We further apply our model for different dimensions, $D = 5, 7, 9, 11, 13, 15$. For each case, we discretize the state space by dividing the relative phases of the base states between 0 and π into 30 partitions. Therefore, for the D-dimensional case, there are $30(D-1)$ categories. The results are shown in Figs. 5(c) and 5(d). The loss and the accuracy of the validation set converge to stable values after about epoch 50. It is worth noting that our approach also allows for stacked classifications

across different dimensions, accommodating up to 1680 distinct classifications for all seven dimensions, from $D = 3$ to $D = 15$. The accuracies for different dimensions are 99.33%, 99.23%, 99.02%, 99.18%, 99.05%, 99.15%, and 99.25%, respectively, from $D = 3$ to $D = 15$. It is evident that the accuracy does not depend on the dimensions. As the dimensions grows, the accuracy maintains high. Therefore, our method can be generalized to the case of high-dimension space.

To validate the applicability of our model, we apply the NNW model to an image transmission task. We aim to transmit a gray image of resolution 100×100. We utilize the OAM states in a nine-dimensional space, thus there are 240 categories in such a space. To map the categories onto the pixel values of the image, the pixel values of the image are normalized between 0 and 239. Each pixel value corresponds to a category associated with a specific phase interval. Experimentally, for each pixel value, we randomly generate an OAM state in the corresponding category as the information carrier. Then the CCD camera captures the image and the image is input to the model as the test data. The pixel value is decoded by predicting which category the image belongs to. This process is repeated 10000 times for all the pixels. The mapping process is detailed in Fig. 6, Our model has demonstrated an exceptional ability to accurately predict the OAM category for each pixel, achieving an accuracy of 99.58%, highlighting the model's robust predictive capabilities and its effectiveness in decoding and reconstructing images from OAM-categorized data. The reconstructed images exhibit a high degree of visual fidelity to the originals. These results not only validate the efficiency of our model but also confirm its potential for practical applications in the field of optical communication.

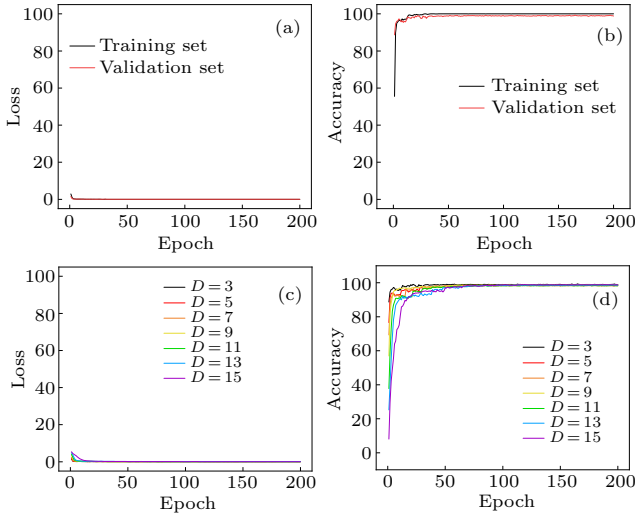


Fig. 5. The loss (a) and the accuracy (b) in each epoch for the training and the validation sets in 3D case. The loss (c) and the accuracy (d) in each epoch for the validation sets at different dimensions.

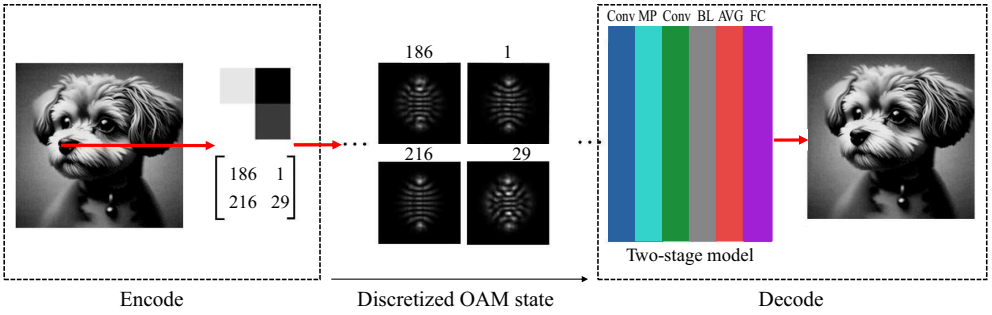


Fig. 6. Procedure of an image transmission task. We map each pixel value of the image to the corresponding category of OAM states, and feed this data into our NNW model for prediction.

4. Conclusion

We have developed a method for OAM state recognition, by discretizing the state space of the transverse spatial modes of structured light and specifically designing a tailored neural network architecture. We consider the combination of the azimuthal and radial indexes of LG modes, which fully describe the transverse spatial modes of structured light. As a result, the LG modes transmit stably in free space. For the OAM states in each category, we assign them with the same classical information. Therefore, our method is robust to the deviation in the generating process of the spatial modes.

The constructed neural network model, based on an enhanced ResNet50 architecture, achieves an accuracy of 99.33% to classify the OAM states for the 3D case and an accuracy of 99.25% for the fifteen-dimensional case. The accuracy maintains a high value for different dimensions. Furthermore, our exploration of image transmission using this model with low OAM number has also yielded positive outcomes, highlighting its practical value in high-capacity optical communication applications. These advances open up new avenues for information transmission and contribute significantly to the field of optical communication and data encoding technology.

Acknowledgements

Project supported by the National Natural Science Foundation of China (Grant Nos. 12204312, 12104190, and U21A20436), the Natural Science Foundation of Jiangxi Province, China (Grant Nos. 20224BAB211014 and 20232BAB201042), the Natural Science Foundation

of Jiangsu Province, China (Grant No. BK20210874), the General Project of Natural Science Research in Colleges and Universities of Jiangsu Province, China (Grant No. 20KJB140008), the Innovation Program for Quantum Science and Technology (Grant No. 2021ZD0301705), and the China Postdoctoral Science Foundation (Grant No. 2021M702628).

References

[1] Cerf N J, Bourennane M, Karlsson A and Gisin N 2002 *Phys. Rev. Lett.* **88** 127902
[2] Chen D X, Liu R F, Zhang P, Wang Y L, Li H R, Gao H and Li F L 2017 *Chin. Phys. B* **26** 060305
[3] Dixon P B, Howland G A, Schneeloch J and Howell J C 2012 *Phys. Rev. Lett.* **108** 143603
[4] Cozzolino D, Bacco D, Da Lio B, Ingerslev K, Ding Y, Dalgaard K, Kristensen P, Galili M, Rottwitt K, Ramachandran S and Oxenløwe L K 2019 *Phys. Rev. Appl.* **11** 064058
[5] Bouchard F, Fickler R, Boyd R W and Karimi E 2017 *Sci. Adv.* **3** e1601915
[6] Hu X M, Xing W B, Liu B H, He D Y, Cao H, Guo Y, Zhang C, Zhang H, Huang Y F, Li C F and Guo G C 2020 *Optica* **7** 738
[7] Vértesi T, Pironio S and Brunner N 2010 *Phys. Rev. Lett.* **104** 060401
[8] Weiss W, Benenti G, Casati G, Guarneri I, Calarco T, Paternostro M and Montangero S 2016 *New J. Phys.* **18** 013021
[9] Fonseca A, de Rosier A, Vértesi T, Laskowski W and Parisio F 2018 *Phys. Rev. A* **98** 042105
[10] Fickler R, Campbell G, Buchler B, Lam P K and Zeilinger A 2016 *Proc. Natl. Acad. Sci. USA* **113** 13642
[11] Sztul H I and Alfano R R 2006 *Opt. Lett.* **31** 999
[12] Berkhout G C G and Beijersbergen M W 2008 *Phys. Rev. Lett.* **101** 100801
[13] Guo C S, Lu L L and Wang H T 2009 *Opt. Lett.* **34** 3686
[14] Hickmann J M, Fonseca E J S, Soares W C and Chávez-Cerda S 2010 *Phys. Rev. Lett.* **105** 053904
[15] Leach J, Padgett M J, Barnett S M, Franke-Arnold S and Courtial J 2002 *Phys. Rev. Lett.* **88** 257901
[16] Berkhout G C G, Lavery M P J, Courtial J, Beijersbergen M W and Padgett M J 2010 *Phys. Rev. Lett.* **105** 153601
[17] Chen D X, Zhang P, Liu R F, Li H R, Gao H and Li F L 2015 *Phys. Lett. A* **379** 2530
[18] Babazadeh A, Erhard M, Wang F, Malik M, Nouroozi R, Krenn M and Zeilinger A 2017 *Phys. Rev. Lett.* **119** 180510
[19] Wen Y, Chremmos I, Chen Y, Zhu J, Zhang Y and Yu S 2018 *Phys. Rev. Lett.* **120** 193904
[20] Brandt F, Hiekkamäki M, Bouchard F, Huber M and Fickler R 2020 *Optica* **7** 98
[21] Chen D X, Wang Y, Wang F, Zhao J L and Yang C P 2023 *Laser Photon. Rev.* **17** 2300277
[22] Chen Z Y and Pu J X 2009 *Chin. Phys. Lett.* **26** 034202
[23] zhou Cui X, li Yin X, Chang H, chao Zhang Z, Jun Wang Y and hua Wu G 2017 *Chin. Phys. B* **26** 114207
[24] Wang J, Yang J Y, Fazal I M, Ahmed N, Yan Y, Huang H, Ren Y, Yue Y, Dolinar S, Tur M and E Willner A 2012 *Nat. Photon.* **6** 488
[25] Bozinovic N, Yue Y, Ren Y, Tur M, Kristensen P, Huang H, Willner A E and Ramachandran S 2013 *Science* **340** 1545
[26] Yan Y, Xie G, Lavery M P, Huang H, Ahmed N, Bao C, Ren Y, Cao Y, Li L, Zhao Z, F Molisch A, Tur M, J Padgett M and E Willner A 2014 *Nat. Commun.* **5** 4876
[27] Zhang L F, Lin Y Y, She Z Y, Huang Z H, Li J Z, Luo X, Yan H, Huang W, Zhang D W and Zhu S L 2021 *Phys. Rev. A* **104** 053525
[28] Giordani T, Suprano A, Polino E, Acanfora F, Innocenti L, Ferraro A, Paternostro M, Spagnolo N and Sciarrino F 2020 *Phys. Rev. Lett.* **124** 160401
[29] Avramov-Zamurovic S, Esposito J M and Nelson C 2023 *J. Opt. Soc. Am. A* **40** 64
[30] da Silva B P, Marques B A D, Rodrigues R B, Ribeiro P H S and Khoury A Z 2021 *Phys. Rev. A* **103** 063704
[31] Guo H, Qiu X and Chen L 2022 *Phys. Rev. Appl.* **17** 054019
[32] Zia D, Checchinato R, Suprano A, Giordani T, Polino E, Innocenti L, Ferraro A, Paternostro M, Spagnolo N and Sciarrino F 2023 *Phys. Rev. Res.* **5** 013142
[33] Li J, Zhang M, Wang D, Wu S and Zhan Y 2018 *Opt. Express* **26** 10494
[34] Liu J, Wang P, Zhang X, He Y, Zhou X, Ye H, Li Y, Xu S, Chen S and Fan D 2019 *Opt. Express* **27** 16671
[35] Bhusal N, Lohani S, You C, Hong M, Fabre J, Zhao P, Knutson E M, Glasser R T and Magaña-Loaiza O S 2021 *Adv. Quantum Technol.* **4** 2000103
[36] Na Y and Ko D K 2021 *Sci. Rep.* **11** 23505
[37] Wang H, Zhan Z, Shen Y, Hu J, Fu X and Liu Q 2022 *Opt. Express* **30** 29781
[38] Liu Z, Yan S, Liu H and Chen X 2019 *Phys. Rev. Lett.* **123** 183902
[39] Na Y and Ko D K 2021 *Sci. Rep.* **11** 2678
[40] Cao M, Yin Y, Zhou J, Tang J, Cao L, Xia Y and Yin J 2021 *Appl. Phys. Lett.* **119** 141103
[41] Zhou J, Yin Y, Tang J, Ling C, Cao M, Cao L, Liu G, Yin J and Xia Y 2022 *Phys. Rev. A* **106** 013519
[42] Chen S, Xie Z, Ye H, Wang X, Guo Z, He Y, Li Y, Yuan X and Fan D 2021 *Light: Sci. Appl.* **10** 222
[43] Zhan H C, Chen B, Peng Y X, Wang L, Wang W N and Zhao S M 2023 *Chin. Phys. B* **32** 044208
[44] Xu P, Tong X, Zeng Z, Liu S and Zhao D 2024 *Chin. Phys. Lett.* **41** 074201
[45] Beijersbergen M, Allen L, van der Veen H and Woerdman J 1993 *Opt. Commun.* **96** 123
[46] Egmont-Petersen M, de Ridder D and Handels H 2002 *Pattern Recognition* **35** 2279
[47] Targ S, Almeida D and Lyman K 2016 arXiv:1603.08029
[48] Srinivas A, Lin T Y, Parmar N, Shlens J, Abbeel P and Vaswani A 2021 2021 *IEEE/CVF Conference on Computer Vision and Pattern Recognition (CVPR)* p. 16514